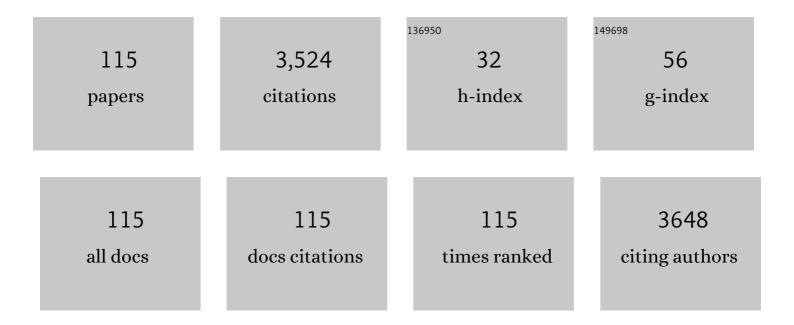
List of Publications by Year in descending order

Source: https://exaly.com/author-pdf/5668065/publications.pdf Version: 2024-02-01



#	Article	IF	CITATIONS
1	Discrimination of Biomass-Burning Smoke From Clouds Over the Ocean Using MODIS Measurements. IEEE Transactions on Geoscience and Remote Sensing, 2022, 60, 1-10.	6.3	0
2	Stability evaluation of tidal flats based on time-series satellite images: A case study of the Jiangsu central coast, China. Estuarine, Coastal and Shelf Science, 2022, 264, 107697.	2.1	10
3	Overwintering fires rising in eastern Siberia. Environmental Research Letters, 2022, 17, 045005.	5.2	16
4	Optical quantification of oil emulsions in multi-band coarse-resolution imagery using a lab-derived HSV model. Marine Pollution Bulletin, 2022, 178, 113640.	5.0	6
5	Chronic oiling in global oceans. Science, 2022, 376, 1300-1304.	12.6	76
6	Evaluation of China's High-Speed Rail Station Development and Nearby Human Activity Based on Nighttime Light Images. International Journal of Environmental Research and Public Health, 2021, 18, 557.	2.6	3
7	Optical Remote Sensing of Oil Spills in the Ocean: What Is Really Possible?. Journal of Remote Sensing, 2021, 2021, .	6.7	41
8	River body extraction from sentinel-2A/B MSI images based on an adaptive multi-scale region growth method. Remote Sensing of Environment, 2021, 255, 112297.	11.0	23
9	Plant species classification in salt marshes using phenological parameters derived from Sentinel-2 pixel-differential time-series. Remote Sensing of Environment, 2021, 256, 112320.	11.0	52
10	Detecting high-temperature anomalies from Sentinel-2 MSI images. ISPRS Journal of Photogrammetry and Remote Sensing, 2021, 177, 174-193.	11.1	16
11	Quantifying ocean surface oil thickness using thermal remote sensing. Remote Sensing of Environment, 2021, 261, 112513.	11.0	21
12	A Quick Band-to-Band Mis-Registration Detection Method for Sentinel-2 MSI Images. Remote Sensing, 2021, 13, 3351.	4.0	2
13	Active Fire Dynamics in the Amazon: New Perspectives From Highâ€Resolution Satellite Observations. Geophysical Research Letters, 2021, 48, e2021GL093789.	4.0	8
14	Satellite Observation of the Marine Light-Fishing and Its Dynamics in the South China Sea. Journal of Marine Science and Engineering, 2021, 9, 1394.	2.6	6
15	Proliferation of offshore wind farms in the North Sea and surrounding waters revealed by satellite image time series. Renewable and Sustainable Energy Reviews, 2020, 133, 110167.	16.4	18
16	Trajectory of coastal wetland vegetation in Xiangshan Bay, China, from image time series. Marine Pollution Bulletin, 2020, 160, 111697.	5.0	16
17	Estimating offshore oil production using DMSP-OLS annual composites. ISPRS Journal of Photogrammetry and Remote Sensing, 2020, 165, 152-171.	11.1	9
18	Optical interpretation of oil emulsions in the ocean – Part II: Applications to multi-band coarse-resolution imagery. Remote Sensing of Environment, 2020, 242, 111778.	11.0	43

#	Article	IF	CITATIONS
19	Global proliferation of offshore gas flaring areas. Journal of Maps, 2020, 16, 396-404.	2.0	13
20	A Predictive Strategy for Mapping Locations Where Future MOSSFA Events Are Expected. , 2020, , 355-368.		3
21	Space eye on flying aircraft: From Sentinel-2 MSI parallax to hybrid computing. Remote Sensing of Environment, 2020, 246, 111867.	11.0	16
22	Onshore-offshore wind energy resource evaluation based on synergetic use of multiple satellite data and meteorological stations in Jiangsu Province, China. Frontiers of Earth Science, 2019, 13, 132-150.	2.1	22
23	Understanding the Spatial-Temporal Patterns and Influential Factors on Air Quality Index: The Case of North China. International Journal of Environmental Research and Public Health, 2019, 16, 2820.	2.6	19
24	Coral reef geomorphology of the Spratly Islands: A simple method based on time-series of Landsat-8 multi-band inundation maps. ISPRS Journal of Photogrammetry and Remote Sensing, 2019, 157, 137-154.	11.1	29
25	Optical interpretation of oil emulsions in the ocean – Part I: Laboratory measurements and proof-of-concept with AVIRIS observations. Remote Sensing of Environment, 2019, 230, 111183.	11.0	46
26	Spatiotemporal variation and socioeconomic drivers of air pollution in China during 2005–2016. Journal of Environmental Management, 2019, 245, 66-75.	7.8	98
27	Using Time-Series HSI Mapping to Determine Ecological Processes and Driving Forces of Red-Crowned Crane (Grus japonensis) Habitat in the Yancheng Biosphere Reserve (China). Journal of Coastal Research, 2019, 35, 322.	0.3	3
28	Evolution of the topography of tidal flats and sandbanks along the Jiangsu coast from 1973 to 2016 observed from satellites. ISPRS Journal of Photogrammetry and Remote Sensing, 2019, 150, 27-43.	11.1	49
29	Seasonal and Intra-Annual Patterns of Sedimentary Evolution in Tidal Flats Impacted by Laver Cultivation along the Central Jiangsu Coast, China. Applied Sciences (Switzerland), 2019, 9, 522.	2.5	5
30	Morphological Characteristics of Tidal Creeks in the Central Coastal Region of Jiangsu, China, Using LiDAR. Remote Sensing, 2019, 11, 2426.	4.0	15
31	Geometric accuracy of remote sensing images over oceans: The use of global offshore platforms. Remote Sensing of Environment, 2019, 222, 244-266.	11.0	25
32	Uncertainty in the optical remote estimation of the biomass of Ulva prolifera macroalgae using MODIS imagery in the Yellow Sea. Optics Express, 2019, 27, 18620.	3.4	11
33	Assessment of offshore oil/gas platform status in the northern Gulf of Mexico using multi-source satellite time-series images. Remote Sensing of Environment, 2018, 208, 63-81.	11.0	32
34	Tracking an Oil Tanker Collision and Spilled Oils in the East China Sea Using Multisensor Day and Night Satellite Imagery. Geophysical Research Letters, 2018, 45, 3212-3220.	4.0	52
35	Identifying industrial heat sources using time-series of the VIIRS Nightfire product with an object-oriented approach. Remote Sensing of Environment, 2018, 204, 347-365.	11.0	62
36	Determining spectral groups to distinguish oil emulsions from Sargassum over the Gulf of Mexico using an airborne imaging spectrometer. ISPRS Journal of Photogrammetry and Remote Sensing, 2018, 146, 251-259.	11.1	24

#	Article	IF	CITATIONS
37	Evolution of Landscape Ecological Risk at the Optimal Scale: A Case Study of the Open Coastal Wetlands in Jiangsu, China. International Journal of Environmental Research and Public Health, 2018, 15, 1691.	2.6	54
38	Distinguishing Anthropogenic CO <sub>2</sub> Emissions From Different Energy Intensive Industrial Sources Using OCOâ€2 Observations: A Case Study in Northern China. Journal of Geophysical Research D: Atmospheres, 2018, 123, 9462-9473.	3.3	36
39	Potential Impacts of China 2030 High-Speed Rail Network on Ground Transportation Accessibility. Sustainability, 2018, 10, 1270.	3.2	31
40	An alternative approach to determine critical angle of contrast reversal and surface roughness of oil slicks under sunglint. International Journal of Digital Earth, 2018, 11, 972-979.	3.9	10
41	A study of the environmental factors influencing the growth phases of Ulva prolifera in the southern Yellow Sea, China. Marine Pollution Bulletin, 2018, 135, 1016-1025.	5.0	30
42	Classification mapping of salt marsh vegetation by flexible monthly NDVI time-series using Landsat imagery. Estuarine, Coastal and Shelf Science, 2018, 213, 61-80.	2.1	69
43	Identification of typical diurnal patterns for clear-sky climatology of surface urban heat islands. Remote Sensing of Environment, 2018, 217, 203-220.	11.0	80
44	Refined use of AISA band-differences for oil slick identification beyond brightness contrast reversal under sunglint. Optics Express, 2018, 26, 33748.	3.4	4
45	Thermal Infrared Contrast Between Different Types of Oil Slicks on Top of Water Bodies. IEEE Geoscience and Remote Sensing Letters, 2017, 14, 1042-1045.	3.1	8
46	Using remote sensing to detect the polarized sunglint reflected from oil slicks beyond the critical angle. Journal of Geophysical Research: Oceans, 2017, 122, 6342-6354.	2.6	16
47	Positive or Negative? Urbanizationâ€Induced Variations in Diurnal Skinâ€6urface Temperature Range Detected Using Satellite Data. Journal of Geophysical Research D: Atmospheres, 2017, 122, 13,229.	3.3	11
48	A review of supervised object-based land-cover image classification. ISPRS Journal of Photogrammetry and Remote Sensing, 2017, 130, 277-293.	11.1	620
49	Saltmarshes Response to Human Activities on a Prograding Coast Revealed by a Dual-Scale Time-Series Strategy. Estuaries and Coasts, 2017, 40, 522-539.	2.2	11
50	Automated Extraction and Mapping for Desert Wadis from Landsat Imagery in Arid West Asia. Remote Sensing, 2016, 8, 246.	4.0	6
51	Survey of reefs based on Landsat 8 operational land imager (OLI) images in the Nansha Islands, South China Sea. Acta Oceanologica Sinica, 2016, 35, 11-19.	1.0	11
52	A strategy for parallelising polygon rasterisation algorithms using multi-core CPUs. Journal of Spatial Science, 2016, 61, 47-68.	1.5	5
53	Hierarchical Filtering Strategy for Registration of Remote Sensing Images of Coral Reefs. IEEE Journal of Selected Topics in Applied Earth Observations and Remote Sensing, 2016, 9, 3304-3313.	4.9	4
54	Accessibility impact of the present and future high-speed rail network: A case study of Jiangsu Province, China. Journal of Transport Geography, 2016, 54, 161-172.	5.0	94

#	Article	IF	CITATIONS
55	Satellite data lift the veil on offshore platforms in the South China Sea. Scientific Reports, 2016, 6, 33623.	3.3	12
56	Use of isochrone maps to assess the impact of high-speed rail network development on journey times: a case study of Nanjing city, Jiangsu province, China. Journal of Maps, 2016, 12, 514-519.	2.0	6
57	Automatic extraction of offshore platforms using time-series Landsat-8 Operational Land Imager data. Remote Sensing of Environment, 2016, 175, 73-91.	11.0	37
58	Erosion and deposition within Poyang Lake: evidence from a decade of satellite data. Journal of Great Lakes Research, 2016, 42, 364-374.	1.9	18
59	Classification mapping and species identification of salt marshes based on a short-time interval NDVI time-series from HJ-1 optical imagery. International Journal of Applied Earth Observation and Geoinformation, 2016, 45, 27-41.	2.8	46
60	River Detection in Remotely Sensed Imagery Using Gabor Filtering and Path Opening. Remote Sensing, 2015, 7, 8779-8802.	4.0	50
61	Training set size, scale, and features in Geographic Object-Based Image Analysis of very high resolution unmanned aerial vehicle imagery. ISPRS Journal of Photogrammetry and Remote Sensing, 2015, 102, 14-27.	11.1	164
62	Analysis of Jiangsu tidal flats reclamation from 1974 to 2012 using remote sensing. China Ocean Engineering, 2015, 29, 143-154.	1.6	25
63	Urban land growth in eastern China: a general analytical framework based on the role of urban micro-agents' adaptive behavior. Regional Environmental Change, 2015, 15, 695-707.	2.9	7
64	Automated extraction of tidal creeks from airborne laser altimetry data. Journal of Hydrology, 2015, 527, 1006-1020.	5.4	21
65	Robustness assessment of urban rail transit based on complex network theory: A case study of the Beijing Subway. Safety Science, 2015, 79, 149-162.	4.9	199
66	Landsat 8 OLI image based terrestrial water extraction from heterogeneous backgrounds using a reflectance homogenization approach. Remote Sensing of Environment, 2015, 171, 14-32.	11.0	123
67	Data decomposition method for parallel polygon rasterization considering load balancing. Computers and Geosciences, 2015, 85, 196-209.	4.2	7
68	River Delineation from Remotely Sensed Imagery Using a Multi-Scale Classification Approach. IEEE Journal of Selected Topics in Applied Earth Observations and Remote Sensing, 2014, 7, 4726-4737.	4.9	36
69	The reconstruction of abnormal segments in HJ-1A/B NDVI time series using MODIS: a statistical method. International Journal of Remote Sensing, 2014, 35, 7991-8007.	2.9	4
70	Study on water conservation value assessment of land ecosystems in Guanzhong-Tianshui Economic Zone. , 2014, , .		0
71	Evaluation of wind energy resources and wind power generation based on SAR-retrieved wind in the eastern sea area of Yancheng, Jiangsu, China. , 2014, , .		0
72	Automatic coral island segmentation based on region-based multi-phase level set method: A case study on Pattle Island, South China Sea. , 2014, , .		0

#	Article	IF	CITATIONS
73	Safety assessment of shipping routes in the South China Sea based on the fuzzy analytic hierarchy process. Safety Science, 2014, 62, 46-57.	4.9	95
74	Automatic Registration of Coastal Remotely Sensed Imagery by Affine Invariant Feature Matching with Shoreline Constraint. Marine Geodesy, 2014, 37, 32-46.	2.0	8
75	Parallel relative radiometric normalisation for remote sensing image mosaics. Computers and Geosciences, 2014, 73, 28-36.	4.2	29
76	Spatiotemporal dynamics of the urban sprawl in a typical urban agglomeration: a case study on Southern Jiangsu, China (1983–2007). Frontiers of Earth Science, 2014, 8, 490-504.	2.1	22
77	Extraction of mangrove in Hainan Dongzhai Harbor based on CART decision tree. , 2014, , .		2
78	Seasonal Pattern of Tidal-Flat Topography along the Jiangsu Middle Coast, China, Using HJ-1 Optical Images. Wetlands, 2013, 33, 871-886.	1.5	30
79	Progress in Marine Oil Spill Optical Remote Sensing: Detected Targets, Spectral Response Characteristics, and Theories. Marine Geodesy, 2013, 36, 334-346.	2.0	48
80	Registration of Mars remote sensing images under the crater constraint. Planetary and Space Science, 2013, 85, 13-23.	1.7	8
81	Integration of LiDAR data and optical multi-view images for 3D reconstruction of building roofs. Optics and Lasers in Engineering, 2013, 51, 493-502.	3.8	42
82	Building region derivation from LiDAR data using a reversed iterative mathematic morphological algorithm. Optics Communications, 2013, 286, 244-250.	2.1	32
83	Using Construction Expansion Regulation Zones to Manage Urban Growth in Hefei City, China. Journal of the Urban Planning and Development Division, ASCE, 2013, 139, 62-69.	1.7	24
84	Fusion of laser scanning data and optical high-resolution imagery for accurate building boundary derivation. Journal of Applied Remote Sensing, 2013, 7, 073570.	1.3	2
85	Invariant triangle-based stationary oil platform detection from multitemporal synthetic aperture radar data. Journal of Applied Remote Sensing, 2013, 7, 073537.	1.3	16
86	Semi-Automatic Registration of Airborne and Terrestrial Laser Scanning Data Using Building Corner Matching with Boundaries as Reliability Check. Remote Sensing, 2013, 5, 6260-6283.	4.0	61
87	Quantitative Analysis of the Waterline Method for Topographical Mapping of Tidal Flats: A Case Study in the Dongsha Sandbank, China. Remote Sensing, 2013, 5, 6138-6158.	4.0	42
88	Topographic Mapping of Offshore Sandbank Tidal Flats Using the Waterline Detection Method: A Case Study on the Dongsha Sandbank of Jiangsu Radial Tidal Sand Ridges, China. Marine Geodesy, 2012, 35, 362-378.	2.0	29
89	Thematic maps for county-level land use planning in Contemporary China. Journal of Maps, 2012, 8, 185-188.	2.0	9
90	Remote sensing image matching by integrating affine invariant feature extraction and RANSAC. Computers and Electrical Engineering, 2012, 38, 1023-1032.	4.8	34

IF # ARTICLE CITATIONS Toward a Method of Constructing Tidal Flat Digital Elevation Models with MODIS and Medium-Resolution Satellite Images. Journal of Coastal Research, 2012, 29, 438. Robust segmentation of building points from airborne LiDAR data and imagery., 2011,,. 92 3 3D Building Model Reconstruction from Multi-view Aerial Imagery and Lidar Data. Photogrammetric 96 Engineering and Remote Sensing, 2011, 77, 125-139. A new method of restoring ETM+ SLC-off images based on multi-temporal images., 2011, , . 94 5 A self-adaptive homomorphic filter method for removing thin cloud., 2011, , . 96 Coastline monitoring with CEBERS 02B HR high-resolution data., 2011, , . 0 Extraction of sandbank shoreline of Jiangsu based on wavelet transformation., 2011,,. Dynamic triangle — Based method for 3D building rooftop reconstruction from LiDAR data., 98 3 2Ó11,,. An image segmentation algorithm for SAR images based on wavelet packets frame transformation. , 2010, , . Simulation and modeling of elevation variations of radial sand banks in Jiangsu province based on 100 0 spatio-temporal correlation analysis., 2010, , Multi-scale urban land cover extraction based on object oriented analysis., 2010, , . 102 Application of Adaboost based ensemble SVM on IKONOS image classification., 2010,,. 0 Multi-points fast marching: A novel method for road extraction., 2010, , . Automatic waterline pick-up based on improved embedded confidence., 2010, , . 104 0 Driving forces analysis of land use change/cover in hilly area of western Zhejiang province: A Case Study in Chun'an County., 2009, , . Post-earthquake assessment of building damage degree using LiDAR data and imagery. Science in China 106 0.9 53 Series D: Earth Sciences, 2008, 51, 133-143. Urban land use change detection through spatial statistical analysis using multi-temporal remote 0.8 sensing data. Proceedings of SPIE, 2008, , . Study on decision-making flow model of high quality prime farmland planning. Proceedings of SPIE, 108 0.8 0 2008, , .

YONGXUE LIU

#	Article	IF	CITATIONS
109	A fast preprocessing algorithm for massive MODIS 1B data. Proceedings of SPIE, 2007, , .	0.8	1
110	An overview of the methods of GIS-based land-use suitability analysis. Proceedings of SPIE, 2007, 6754, 1110.	0.8	9
111	Research on scenario simulation of land-use planning based on CA model: A case study in Kunming metropolitan area. Proceedings of SPIE, 2007, , .	0.8	0
112	Tidal flat stability analysis based on GIS & RS technology: a case study in Dongsha sandbank, offshore the coast of Jiangsu province. , 2007, , .		1
113	Multi-flow direction algorithms for extracting drainage network based on digital elevation model. , 2007, , .		1
114	Classification of Landsat 7 ETM+ imagery in western mountainous area of Zhejiang based on gray-gradient co-concurrency matrix. Proceedings of SPIE, 2007, , .	0.8	0
115	Review of remotely sensed imagery classification patterns based on object-oriented image analysis. Chinese Geographical Science, 2006, 16, 282-288.	3.0	35